Structure and properties of reduced barium niobium oxide single crystals obtained from borate fluxes

ARTICLE *in* CHEMINFORM · MAY 1991

Impact Factor: 0.74 · DOI: 10.1021/cm00015a031

5 AUTHORS, INCLUDING:

A. T. Fiory
New Jersey Institute of Technology
212 PUBLICATIONS **6,018** CITATIONS

Structure and Properties of Reduced Barium Niobium Oxide Single Crystals Obtained from Borate Fluxes

B. Hessen,* S. A. Sunshine,* T. Siegrist, A. T. Fiory, and J. V. Waszczak

AT&T Bell Laboratories, 600 Mountain Avenue, Murray Hill, New Jersey 07974

Received January 2, 1991. Revised Manuscript Received March 4, 1991

Single crystals of the reduced niobate $Ba_2Nb_{15}O_{32}$ are produced by heating NbO_2 in $BaO{\cdot}3B_2O_3$ under high-vacuum conditions. The borate acts both as a source of BaO and as a flux for crystallization. The compound $Ba_2Nb_{15}O_{32}$ crystallizes in space group $R\bar{3}$ (a = 7.777 (1) Å, c = 35.518 (6) Å) and contains isolated $[Nb_6O_{12}]O_6$ clusters arranged in layers. As side products, single crystals of the following phases are formed: $Ba_3Nb_5O_{15}$ (space group $P4/mbm$, a = 12.598 (1) Å, c = 3.9774 (5) Å), with a tetragonal tungsten bronze-type structure, and $BaNb_8O_{14}$ (space group $Pcab$, a = 9.4222 (9) Å, b = 10.3649 (9) Å, c = 23.716 (3) Å), which contains $[Nb_6O_{12}]O_6$ clusters in a three-dimensional arrangement, interconnected by three different modes of oxygen sharing. The new compound $Ba_2Nb_{15}O_{32}$ exhibits a semiconductor-to-semiconductor transition at 170 K, coinciding with a transition from a weakly paramagnetic state to diamagnetism. Single-crystal resistivity measurements on $Ba_3Nb_5O_{15}$ indicate a significant anisotropy ($\rho_{\perp c} = 55\ \rho_{\parallel c}$ at 300 K) and small bandgap semiconducting behavior.

Introduction

Reduced ternary oxides of the early transition metals form a class of compounds that exhibit interesting electronic properties. For example, charge density wave (CDW) driven metal-to-semiconductor transitions are observed in the "blue bronzes" $A_{0.3}MoO_3$ (A = K, Rb, Tl),[1,2] and various reduced ternary oxides exhibit superconductivity, such as the spinel $LiTi_2O_4$[3-5] and some tetragonal and hexagonal tungsten and molybdenum bronzes.[6-8] Very recently evidence for superconductivity in $Li_{0.5}NbO_2$ was reported.[9] Single crystals are desirable for measuring the physical properties of this class of compounds. In systems for which low-melting nonreduced precursors are available (e.g., A_2MO_4 and $A_2M_2O_7$; A = alkali metal, M = Mo, W) molten salt electrolysis is often a convenient way of obtaining single crystals. For other systems (particularly niobates) other methods have to be used. Crystal growth from molten salt fluxes has been extensively employed (for example, for garnets, ferroelectrics, and ferrites),[10] but very rarely for reduced early-transition-metal systems, which require a rigorously inert atmosphere. Alkaline-earth-metal borate fluxes seem to be suitable for this purpose, being redox neutral and exhibiting low volatility, allowing their use under high-vacuum conditions. They can also act as source or buffer for the alkaline-earth-metal oxide that is part of the ternary system. Here we describe the crystallization of reduced barium niobates from the barium borate $BaO{\cdot}3B_2O_3$ under high-vacuum conditions.

The reduced Ba–Nb–O phase diagram has been studied by several investigators and contains a variety of structure types ranging from perovskite[11,12] and tetragonal tungsten bronze (TTB) type[13,14] compounds to more complicated structures such as $Ba_3Nb_8O_{21}$[15] and compounds containing octahedral Nb_6O_{12} clusters.[16-18] Here we report the formation of single crystals of $Ba_2Nb_{15}O_{32}$, $Ba_3Nb_5O_{15}$ (a TTB-type phase prepared earlier as a ceramic[14]), and $BaNb_8O_{14}$, recently reported by Hibble et al.[18] All com-

Table I. X-ray Powder Diffraction Pattern of $Ba_2Nb_{15}O_{32}$ (Cu Kα Radiation), with Indexing Based on the Hexagonal Cell Setting

index	$2\theta_0$	I_0	$2\theta_c$
1 0 1	13.45	11	13.40
1 0 4	16.60	8	16.56
0 1 5	18.23	19	18.20
1 0 7	22.01	10	21.98
0 0 9	22.65	7	22.58
1 1 0	22.95	22	22.92
0 1 8	24.10	60	24.06
-1 2 6	27.53	92	27.50
0 2 4	28.43	100	28.46
2 0 5	29.42	73	29.40
0 0 12	30.30	17	30.26
0 1 11	30.77	40	30.80
1 1 9	32.40	45	32.40
2 0 8	33.45	12	33.48
2 1 1	35.38	91	35.40
2 1 4	36.80	53	36.78
1 2 5	37.59	27	37.60
0 0 15	38.03	12	38.08
2 1 7	39.65	15	39.68
3 0 0	40.15	8	40.22
-1 3 8	40.92	46	40.94
0 3 6	43.13	17	43.16
2 1 10	43.78	41	43.82
2 0 14	44.79	5	44.82
-1 3 11	45.42	18	45.44
0 0 18	45.96	9	46.10
3 0 9	46.60	10	46.62
2 2 3	47.43	5	47.46
2 1 13	48.92	15	49.00
-2 4 6	49.36	17	49.42
-1 3 14	50.86	81	50.90

(1) Greenblatt, M. *Chem. Rev.* **1988**, *88*, 31.
(2) Schlenker, C., Ed. *Low-Dimensional Electronic Properties of Molybdenum Bronzes and Oxides*; Kluwer: Dordrecht, 1989.
(3) Johnston, D. C.; Prakash, H.; Zachariasen, W. H.; Viswanathan, R. *Mater. Res. Bull.* **1973**, *8*, 777.
(4) Harrison, M. R.; Edwards, P. P.; Goodenough, J. B. *Philos. Mag.* **1985**, *52B*, 679.
(5) Ueda, Y.; Tanaka, T.; Kosuge, K.; Ishikawa, M.; Yasuoka, H. *J. Solid State Chem.* **1988**, *77*, 401.
(6) Raub, Ch. J.; Sweedler, A. R.; Jensen, M. A.; Broadston, S.; Matthias, B. T. *Phys. Rev. Lett.* **1964**, *13*, 746.
(7) Sweedler, A. R.; Raub, Ch. J; Matthias, B. T. *Phys. Lett.* **1965**, *15*, 108.
(8) Sleight, A. W.; Bither, T. A.; Biersted, P. E. *Solid State Commun.* **1969**, *7*, 299.
(9) Geselbracht, M. J.; Richardson, T. J.; Stacy, A. M. *Nature* **1990**, *345*, 324.
(10) Elwell, D.; Scheel, H. J. *Crystal Growth from High-Temperature Solutions*; Academic Press: London, 1975.
(11) Kreiser, R.; Ward, A. *J. Solid State Chem.* **1970**, *1*, 368.
(12) Ridgeley, D.; Ward, A. *J. Am. Chem. Soc.* **1955**, *77*, 6132.
(13) Galasso, F.; Katz, L.; Ward, A. *J. Am. Chem. Soc.* **1959**, *81*, 5898.
(14) Feltz, A.; Langbein, H. *Z. Anorg. Allg. Chem.* **1976**, *425*, 47.
(15) Groult, D.; Chailleux, J. M.; Choisnet, J.; Raveau, B. *J. Solid State Chem.* **1976**, *19*, 235.
(16) Svensson, G. *Mater. Res. Bull.* **1988**, *23*, 437.
(17) Svensson, G. *Solid State Ionics* **1989**, *32/33*, 126.
(18) Hibble, S. J.; Cheetham, A. K.; Koehler, J.; Simon, A. *J. Less-Common Met.* **1989**, *154*, 271.

0897-4756/91/2803-0528$02.50/0

Table II. Crystallographic and Experimental Data

	$Ba_2Nb_{15}O_{32}$	$BaNb_8O_{14}$	$Ba_3Nb_5O_{15}$
space group	$R\bar{3}$ (No. 148)	*Pcab* (No. 61)	*P4/mbm* (No. 127)
cryst size, mm	0.15 × 0.15 × 0.10	0.08 × 0.05 × 0.03	0.17 × 0.04 × 0.03
a, Å	7.777 (1)	9.4222 (9)	12.598 (1)
b, Å		10.3649 (9)	
c, Å	35.518 (6)	23.716 (3)	3.9774 (5)
V, Å^3	1860.4 (4)	2316.1 (4)	631.25 (9)
Z	3	8	2
D_c, g/cm^3	5.838	6.335	5.874
μ (Mo, Kα), cm^{-1}	96.0	107.1	134.7
scan type	ω	ω	$\theta/2\theta$
reflns measd	2777	3412	9675
indep reflns	2549	3404	804
obsd reflns ($I > 2.5\sigma(I)$)	1631	2208	709
refined params	50	137	29
R	0.046	0.066	0.026
R_w ($w = 1/\sigma^2(F_o)$)	0.042	0.065	0.030

pounds were characterized by single-crystal X-ray diffraction, and some of their physical properties are discussed.

Experimental Section

Sample Preparation. Single crystals of the reduced niobates $Ba_2Nb_{15}O_{32}$, $BaNb_8O_{14}$, and $Ba_3Nb_5O_{15}$ were obtained as follows: a mixture of NbO_2 (Alfa) and $BaO{\cdot}3B_2O_3$ in a 1:1.3–1.8 molar ratio was placed in a molybdenum-foil boat with a molybdenum-foil lid in a high-temperature vacuum furnace (Centorr). The mixture was heated in vacuo to 400 °C to remove adsorbed water and then heated at 1100 °C (10^{-6}–10^{-7} Torr) for 1 h. Subsequently the mixture was cooled at 8 °C/h to 850 °C, after which the heater was turned off, allowing the sample to cool down to room temperature in 1 h. The glassy flux was removed by etching with a dilute aqueous HF solution. The resulting mixture consists mainly of golden trigonally compressed octahedra and hexagons of $Ba_2Nb_{15}O_{32}$ (up to 0.6-mm diameter). Also present are blue rectangular crystals of $Ba_3Nb_5O_{15}$, with dimensions up to 2 mm long and 0.8 mm wide, and dull-metallic platelets of $BaNb_8O_{14}$ (sometimes arranged in pseudohexagonal multiple twins), accompanied by small crystals of residual NbO_2.

Ceramic samples of $Ba_2Nb_{15}O_{32}$ were prepared by heating a pressed pellet of $BaNb_2O_6$, NbO (Alfa), and NbO_2, with B_2O_3 as a mineralizer, in 2:2:9:1 molar ratio to 1100 °C for 15 h (in vacuum, wrapped in Mo foil). The well-crystallized golden pellet consisted of $Ba_2Nb_{16}O_{32}$ (as identified by its X-ray powder pattern; see Table I) but always contained some NbO_2. Probably, the mineralizer B_2O_3 extracts some of the BaO from the niobate to form barium borates, leaving residual NbO_2. Recrystallization of the ceramic from the $BaO{\cdot}3B_2O_3$ flux also produces single crystals of $Ba_2Nb_{15}O_{32}$.

The $BaO{\cdot}3B_2O_3$ used as a flux was prepared by heating a mixture (1:3 molar ratio) of $Ba(NO_3)_2$ and B_2O_3 (Fisher) in an alumina crucible at 700 °C (ramp rate 200 °C/h) in air for 12 h. The compound $BaNb_2O_6$ was prepared by firing $Ba(CO_3)$ and Nb_2O_5 (Aldrich) together in a Pt crucible in air at 1300 °C as previously described.[19]

X-ray Structure Determinations. All crystals were measured at 23 °C on an Enraf-Nonius CAD-4 diffractometer using graphite-monochromated Mo Kα radiation and the NRCCAD program package.[20] All calculations were carried out on an Alliant FX/80 computer, using the NRCVAX structure package.[21] Lattice parameters were determined from absolute 2θ values of at least 24 reflections at high angles ($50° < 2\theta < 90°$). A Gaussian integration absorption correction was carried out for all the collected intensity data. For $Ba_2Nb_{15}O_{32}$ and $BaNb_8O_{14}$ the metal atom positions were obtained from direct methods. Refinement of $Ba_3Nb_5O_{15}$ was started from the (symmetrized) coordinates reported for $Ba_3TiNb_4O_{15}$.[22] Further experimental and crystallographic data are listed in Table II, atomic coordinates and isotropic thermal parameters in Tables III–V.

Measurement of Physical Properties. To measure the resistivity of $Ba_2Nb_{15}O_{32}$ and $Ba_3Nb_5O_{15}$, silver wires were attached at six positions on single crystals by using Ag paste and In/Ga alloy. Four independent four-probe ac resistance measurements were taken and deconvolved as reported previously[23] to yield the resistivities along the two principal crystal axes. Magnetic susceptibility measurements on a batch of $Ba_2Nb_{15}O_{32}$ crystals were done on a Faraday type instrument. For high-temperature measurements (300–660 K) a sample was sealed under reduced Ar pressure in a quartz tube.

Table III. Atomic Positional Parameters and Isotropic Temperature Factors for $Ba_2Nb_{15}O_{32}$

	x	*y*	*z*	B_{iso}
Ba	0.0	0.0	0.36152 (3)	1.126 (22)
Nb(1)	0.0	0.0	0.0	1.29 (5)
Nb(2)	0.26398 (12)	0.18964 (12)	0.266283 (21)	0.699 (24)
Nb(3)	0.21723 (10)	0.19466 (10)	0.466958 (18)	0.368 (20)
Nb(4)	0.0	0.0	0.13868 (3)	0.475 (24)
O(1)	0.2333 (9)	0.2030 (9)	0.56811 (17)	0.61 (7)
O(2)	0.2389 (9)	0.1651 (9)	0.83333 (18)	0.68 (7)
O(3)	0.0	0.0	0.2379 (3)	0.71 (12)
O(4)	0.2354 (9)	0.1741 (9)	0.10384 (17)	0.62 (7)
O(5)	0.2363 (10)	0.1779 (10)	0.70666 (18)	0.75 (7)
O(6)	0.2053 (10)	−0.0123 (10)	0.03198 (18)	0.80 (7)

Table IV. Atomic Positional Parameters and Isotropic Temperature Factors for $BaNb_8O_{14}$

	x	*y*	*z*	B_{iso}
Ba	0.50637 (12)	0.48807 (11)	0.13528 (5)	0.67 (3)
Nb(1)	0.11769 (15)	0.66554 (14)	0.12420 (6)	0.18 (4)
Nb(2)	0.12470 (15)	0.42339 (14)	0.18318 (6)	0.21 (4)
Nb(3)	0.12573 (15)	0.42433 (14)	0.06684 (6)	0.18 (4)
Nb(4)	0.87508 (16)	0.57873 (15)	0.06619 (6)	0.27 (5)
Nb(5)	0.87626 (15)	0.57299 (14)	0.18214 (6)	0.21 (4)
Nb(6)	0.88107 (15)	0.33765 (14)	0.12012 (6)	0.19 (4)
Nb(7)	0.86169 (17)	0.31556 (15)	0.25332 (6)	0.45 (5)
Nb(8)	0.61699 (16)	0.33974 (15)	0.00139 (6)	0.24 (4)
O(1)	−0.0057 (13)	0.7545 (12)	0.0642 (5)	0.15 (15)
O(2)	0.2508 (13)	0.5964 (12)	0.1884 (5)	0.37 (17)
O(3)	−0.0082 (12)	0.7467 (12)	0.1886 (5)	0.16 (15)
O(4)	0.2579 (13)	0.5850 (11)	0.0619 (5)	0.15 (15)
O(5)	0.7401 (14)	0.6515 (13)	0.1236 (5)	0.57 (18)
O(6)	0.2551 (14)	0.3411 (12)	0.1257 (5)	0.39 (17)
O(7)	−0.0116 (13)	0.4827 (12)	0.2467 (5)	0.30 (16)
O(8)	−0.0078 (13)	0.2615 (12)	0.1891 (5)	0.39 (17)
O(9)	0.2530 (14)	0.3362 (13)	0.2482 (6)	0.64 (18)
O(10)	0.0	0.5	0.0	0.12 (22)
O(11)	0.0087 (14)	0.2458 (13)	0.0611 (5)	0.52 (17)
O(12)	0.2315 (13)	0.3157 (12)	0.0008 (5)	0.39 (17)
O(13)	0.7394 (15)	0.4097 (14)	0.0615 (6)	0.87 (20)
O(14)	0.7574 (13)	0.4072 (12)	0.1879 (5)	0.29 (16)
O(15)	0.5	0.5	0.0	0.6 (3)

Table V. Atomic Positional Parameters and Isotropic Temperature Factors for $Ba_3Nb_5O_{15}$

	x	*y*	*z*	B_{iso}
Ba(1)	0.0	0.0	0.0	0.453 (14)
Ba(2)	0.17064 (4)	0.67064	0.0	1.715 (19)
Nb(1)	0.0	0.5	0.5	0.85 (3)
Nb(2)	0.07663 (4)	0.21355 (4)	0.5	0.375 (16)
O(1)	0.0	0.5	0.0	0.95 (14)
O(2)	0.2815 (4)	0.78152	0.5	0.60 (9)
O(3)	0.0759 (4)	0.2095 (4)	0.0	0.84 (7)
O(4)	0.3442 (4)	0.0074 (4)	0.5	0.74 (6)
O(5)	0.1395 (4)	0.0699 (4)	0.5	0.55 (6)

(19) Francombe, M. H. *Acta Crystallogr.* **1969**, *B13*, 131.
(20) LePage, J.; White, P. S.; Gabe, E. J. *Proc. Am. Crystallogr. Assoc. Annu. Meeting 1986*; Hamilton, Canada; AIP: New York, 1986; Poster PA23.
(21) Gabe, E. J.; LePage, Y.; Charland, J. P.; Lee, F. L.; White, P. S. *J. Appl. Crystallogr.* **1989**, *22*, 384.
(22) Jamieson, P. B.; Abrahams, S. C. *Acta Crystallogr.* **1968**, *B24*, 984.
(23) Martin, S.; Fiory, A. T.; Fleming, R. M.; Schneemeyer, L. F.; Waszczak, J. V. *Phys. Rev. Lett.* **1988**, *60*, 2194.

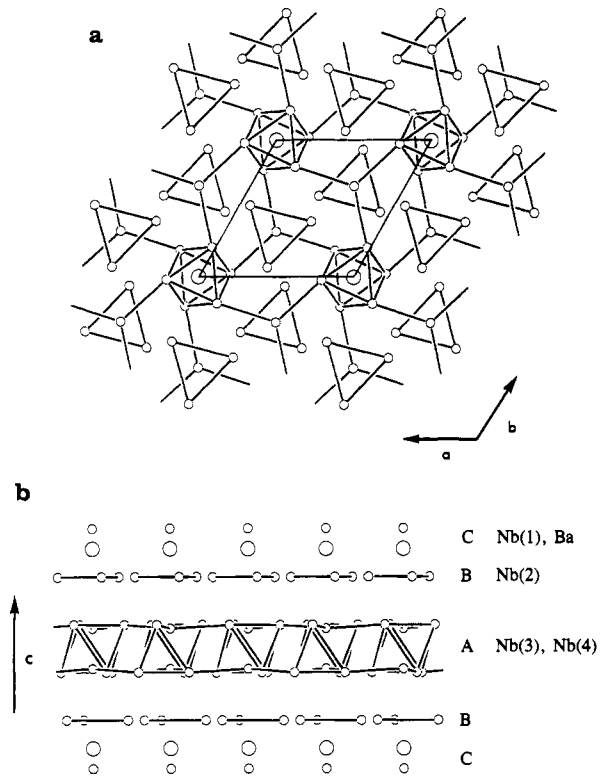

Figure 1. Crystal structure of $Ba_2Nb_{15}O_{32}$ viewed along (a) and perpendicular to (b) the *c* axis. Oxygen atoms omitted for clarity, Nb represented by small, Ba by large circles. Niobium-niobium contacts <3.2 Å drawn to indicate the arrangement in the A layer and the triangular Nb_3O_{13} groups.

Results

The low-melting (750 °C) $BaO{\cdot}3B_2O_3$ proved to be a useful medium to obtain single crystals of several reduced barium niobates. It provides a source of BaO for reaction with NbO_2 and acts as a suitable flux for the growth of single crystals. Heating NbO_2 in $BaO{\cdot}3B_2O_3$ produced three crystalline products, $Ba_2Nb_{15}O_{35}$, $BaNb_8O_{14}$, and $Ba_3Nb_5O_{15}$. In the main product, $Ba_2Nb_{15}O_{32}$, the average niobium oxidation state is +4, and it may be considered as a direct reaction product of BaO and NbO_2. The side products have different average Nb oxidation states: $Nb^{4.8+}$ in $Ba_3Nb_5O_{15}$ and $Nb^{3.5+}$ in $BaNb_8O_{14}$. These products are probably formed by a disproportionation side reaction, but some excess $Ba_3Nb_5O_{15}$ may also arise from some gettering of traces of oxygen and water. The crystals produced were of sufficient quality and size to allow single-crystal X-ray diffraction studies on all three compounds, as well as four-probe single-crystal resistivity measurements on $Ba_2Nb_{15}O_{32}$ and $Ba_3Nb_4O_{15}$.

Description of the Structures

$Ba_2Nb_{15}O_{32}$. The crystal structure of $Ba_2Nb_{15}O_{32}$ is shown in Figure 1, projected both along the *c* axis (a) and perpendicular to it (b). It can be described as consisting of three different layers, A–C, parallel to the *ab* plane, that are interconnected by oxygen sharing. Selected interatomic distances and angles are listed in Table VI. Only one-third of the unit cell along the *c* axis ($0.33 \le z \le 0.67$) is shown in Figure 1. Layer A is built from octahedral Nb_6 clusters of the type $[Nb_6O_{12}]O_6$ (Figure 2), with short intracluster metal–metal distances (Nb(3)–Nb(3′) = 2.787 (1), 2.846 (1) Å). Oxygen atoms bridging edges of the Nb_6 octahedraon are indicated as O^i, terminal oxygens on the corners of the octahedron as O^a. Clusters of this type have been reported for a number of strongly reduced ternary

Table VI. Selected Interatomic Distances (Å) for $Ba_2Nb_{15}O_{32}$, with Estimated Standard Deviations in Parentheses

Ba–O(1)	3.028 (6)	3×	Nb(3)–Nb(3)	2.787 (1)	2×
–O(5)	2.935 (6)	3×		2.846 (1)	2×
	2.965 (6)	3×	–Nb(4)	3.105 (1)	
–O(6)	3.119 (8)	3×	–O(1)	2.10 (1)	
Nb(2)–Nb(2)	3.167 (2)	2×		2.05 (1)	
–O(1)	2.088 (9)		–O(2)	2.106 (6)	
–O(3)	2.093 (5)			2.043 (9)	
–O(4)	1.940 (6)		–O(4)	2.189 (3)	
–O(5)	1.95 (1)		Nb(1)–O(6)	2.001 (6)	6×
	2.05 (1)		Nb(4)–O(2)	1.925 (8)	3×
–O(6)	1.876 (6)			2.059 (8)	3×

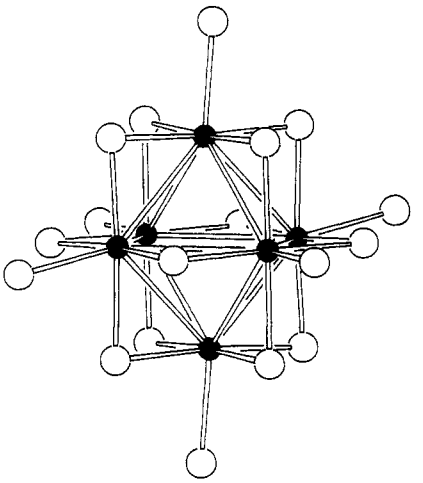

Figure 2. Octahedral $[Nb_6O^i_{12}]O^a_6$ cluster in $Ba_2Nb_{15}O_{32}$. The Nb atoms are shaded; the O^i atoms are bridging the edges of the Nb_6 octahedron; the O^a atoms are the terminal oxygen atoms.

niobates (average Nb oxidation state ≤3.5+).[18,24-31] The $[Nb_6O_{12}]O_6$ clusters in the layer do not share oxygen atoms but are interconnected by a single niobium atom (Nb(4)) in an octahedral hole in the layer, sharing two oxygen atoms with each of the three neighboring $[Nb_6O_{12}]O_6$ clusters (Nb(3)–Nb(4) = 3.105 (1) Å). The adjacent B-layer contains groups of three edge-sharing NbO_6 octahedra forming a Nb_3O_{13} unit. The intermetallic distances within this Nb_3O_{13} unit (Nb(2)–Nb(2′) = 3.176 (1) Å) are significantly longer than those in the Nb_6 cluster, indicating the absence of Nb–Nb interaction. This is in contrast to the isomorphous Nb_3X_{13} group in the reduced Nb halides, β-Nb_3X_8, where significant intermetallic bonding interaction is present.[32] In the absence of intermetallic bonding, the Nb atoms in the Nb_3O_{13} group are displaced away from the group center, making the Nb(2)–O(3) distance (O(3) being the central oxygen) the longest (2.093 (5) Å), and the diametrically opposed Nb(2)–O(6) distance of 1.876 (6) Å the shortest in the group. The C layer contains Ba atoms, located in the hexagonal cuboctahedral cavity created by isolated NbO_6 octahedra (Nb(1)), with Ba–O distances ranging from 2.965 (6) to 3.229 (8) Å. All

(24) Evans, D. M.; Katz, L. *J. Solid State Chem.* **1973**, *6*, 459.
(25) Marinder, R. B. *Chim. Scr.* **1977**, *11*, 197.
(26) Burnus, R.; Koehler, J.; Simon, A. *Z. Naturforsch.* **1987**, *42b*, 536.
(27) Hibble, S. J.; Cheetham, A. K.; Cox, D. E. *Inorg. Chem.* **1987**, *26*, 2389.
(28) Koehler, J.; Simon, A. *Z. Anorg. Allg. Chem.* **1987**, *553*, 106.
(29) Koehler, J.; Miller, G.; Simon, A. *Z. Anorg. Allg. Chem.* **1989**, *568*, 8.
(30) Koehler, J.; Simon, A. *Z. Anorg. Allg. Chem.* **1989**, *572*, 7.
(31) Koehler, J.; Simon, A.; Hibble, S. J.; Cheetham, A. K. *J. Less-Common Met.* **1988**, *142*, 123.
(32) Simon, A.; Von Schnering, H. G. *J. Less-Common Met.* **1966**, *11*, 31.

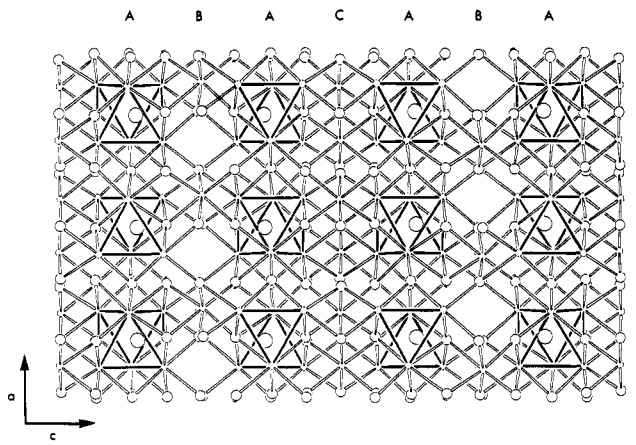

Figure 3. Crystal structure of $BaNb_8O_{14}$ viewed along the *b* axis. The Nb atoms are represented as small; the O atoms as larger circles; the largest circles represent the Ba atoms. Bonds are drawn solid between the Nb atoms in the Nb_6 cluster.

the layers are connected via shared planes of oxygen atoms, producing the stacking sequence $[CBAB]_\infty$.

The absence of Nb–Nb interaction in the Nb_3O_{13} groups indicates a +5 oxidation state for Nb(2) in the structure. The regular octahedral coordination Nb(1) with Nb(1)–O(6) = 2.001 (5) Å also suggests a +5 Nb(1), leaving 15 valence electrons/formula unit to reside in the A layer. As the average Nb(4)–O distance in the layer is within 2 σ of that for Nb(1) (although the octahedron is more distorted), it is likely that the valence electrons are mainly localized in the $[Nb_6O_{12}]O_6$ clusters, providing for Nb–Nb interaction within this cluster. Thus the compound may be formulated in the ionic limit as $Ba_2^{2+}Nb_3^{5+}[Nb_3^{5+}]_2[Nb_6^{2.5+}]O_{32}^{2-}$, with 15 valence electrons in the Nb_6 cluster. This corresponds with the other known $[Nb_6O_{12}]O_6$-containing compounds, usually with 14–15 valence electrons/cluster. The overall oxidation state of Nb in these compounds ranges from +2.7 for $M_3Nb_6O_{11}$ (M = Mg, Mn[26]) to +3.5 for $NaNb_{10}O_{18}$[30] and $Na_3Al_2Nb_{34}O_{64}$.[28] The occurrence of Nb_6 clusters in a compound with an average Nb oxidation state of 4+ indicates that these clusters can act as structural elements and as valence electron reservoirs in more oxidized phases as well, depending on the nature of the layers or groups separating them.

$BaNb_8O_{14}$. A previous single-crystal structure determination of $BaNb_8O_{14}$[18] reported a unit cell with a = 23.80 (1) Å, b = 10.331 (5) Å, c = 9.325 (5) Å with space group *Cmca*. Careful examination of crystals obtained from $BaO{\cdot}3B_2O_3$ flux indicated, however, a primitive unit cell and space group *Pcab*.

A projection of the $BaNb_8O_{14}$ structure along the *b* axis is shown in Figure 3. Selected interatomic distances and angles are listed in Table VII. The structure is built around layers parallel to the *ab* plane containing a network of $[Nb_6O_{12}]O_6$ clusters (Nb(1–6)) that share oxygens in a $[Nb_6O^i_{10}O^{i-a}_{2/2}]O^a_4O^{a-i}_{2/2}$ fashion (O^{i-a} indicates an edge-bridging oxygen O^i of one cluster that acts as a terminal oxygen O^a for another cluster; for further description of the nomenclature used, see ref 33), as well as the barium ions (A layers in Figure 3). These are similar to layers found in $SrNb_8O_{14}$.[31] The structures of the Sr and Ba analogues, however, differ in the interconnection of these layers along the *c* direction. The A layers in $BaNb_8O_{14}$ are stacked together with two different layers, B and C, containing NbO_6 octahedra. These octahedra are isolated in the B layers (Nb(7), $z \approx {}^1/_4, {}^3/_4$), whereas they form corner-sharing pairs in the C layers (Nb(8), $z \approx 0, {}^1/_2$). The stacking sequence of the layers is $[ABAC]_\infty$. The Nb_6 clusters of the A layers interconnect in the *c* direction across the C layer by sharing three oxygens (two O^a, one O^i, as is also observed in $SrNb_8O_{14}$.[31] However, across the B layer the two adjacent A layers are shifted (0, ${}^1/_2$, 0) relative to each other, and each Nb_6 cluster now shares two (O^a) oxygens with two other clusters, while the O^i is not shared. The connectivities of the clusters along the *c* direction are illustrated in Figure 4. Thus $BaNb_8O_{14}$ shows three different ways of interconnecting $[Nb_6O_{12}]O_6$ clusters through oxygen sharing. The connection pattern of the Nb_6 clusters can be described as $[Nb_6O^i_9O^{i-a}_{2/2}O^{i-i}]$-$O^{a-a}_{4/2}O^{a-i}_2$, where there are two different O^{a-a}'s (2:2, across B and across C), and two different O^i's (8:1). The alkaline-earth-metal ion, which is cuboctahedrally coordinated in $SrNb_8O_{14}$ with Sr–O distances from 2.69 to 2.98 Å, now occupies a larger cuboctahedral site, with Ba–O distances from 2.80 to 3.21 Å. The formation of a larger 12-coordinate cavity to accommodate the Ba ion in $BaNb_8O_{14}$ is probably the origin of the structural differences between the Sr and Ba homologues. The average Nb–O distances in the NbO_6 octahedra are nearly equal (2.00–2.01 Å) for Nb(2) and Nb(7) and identical with that found for the NbO_6 octahedron in $SrNb_8O_{14}$. Consequently, $BaNb_8O_{14}$ can be likewise formulated in the ionic limit as Ba^{2+}-

Table VII. Selected Interatomic Distances (Å) for $BaNb_8O_{14}$, with Estimated Standard Deviations in Parentheses

Ba–O(2)	2.94 (1)	Nb(1)–Nb(2)	2.873 (2)
–O(3)	3.02 (1)	–Nb(3)	2.847 (2)
–O(4)	3.08 (1)	–Nb(4)	2.816 (2)
–O(5)	2.79 (1)	–Nb(5)	2.825 (2)
–O(6)	2.82 (1)	Nb(2)–Nb(3)	2.759 (2)
–O(7)	2.81 (1)	–Nb(5)	2.808 (2)
–O(8)	2.89 (1)	–Nb(6)	2.880 (2)
–O(11)	2.99 (1)	Nb(3)–Nb(4)	2.853 (2)
–O(13)	2.92 (1)	–Nb(6)	2.778 (2)
–O(14)	2.80 (1)	Nb(4)–Nb(5)	2.750 (2)
–O(14)	2.92 (1)	–Nb(6)	2.808 (2)
–O(15)	2.84 (1)	Nb(5)–Nb(6)	2.849 (2)
Nb(7)–O(2)	1.96 (1)	Nb(8)–O(1)	2.02 (1)
–O(3)	1.98 (1)	–O(4)	2.01 (1)
–O(7)	2.11 (1)	–O(11)	2.01 (1)
–O(8)	2.03 (1)	–O(12)	1.94 (1)
–O(9)	1.88 (1)	–O(13)	2.02 (1)
–O(14)	2.07 (1)	–O(15)	1.994 (4)

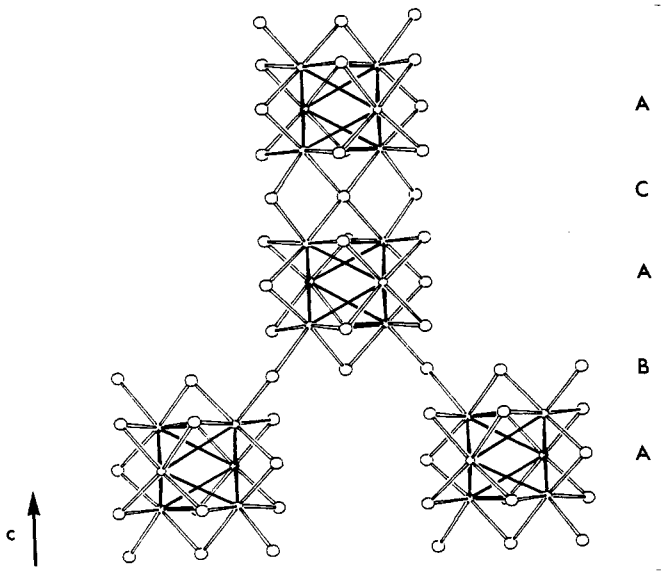

Figure 4. Oxygen sharing arrangement between the $[Nb_6O_{12}]O_6$ clusters in $BaNb_8O_{14}$ in the *z* direction.

(33) Schaefer, H.; Von Schnering, H. G. *Angew. Chem.* **1964**, *76*, 833.

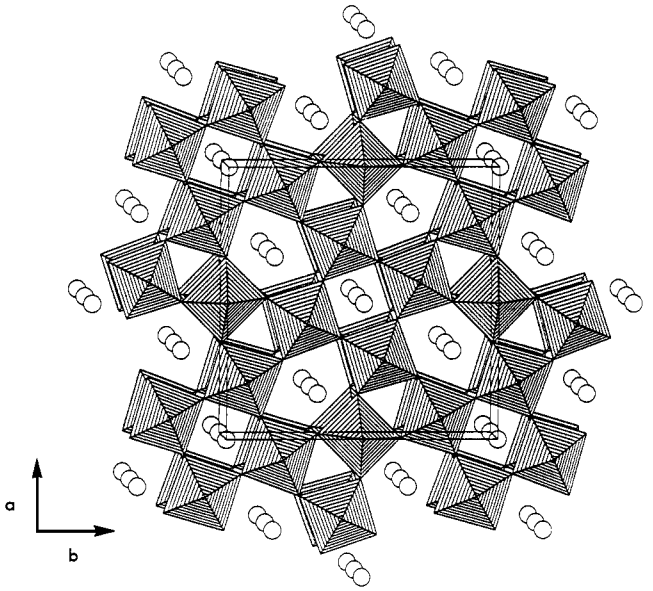

Figure 5. Polyhedral representation of the crystal structure of $Ba_3Nb_5O_{15}$ viewed along the *c* axis. NbO_6 octahedra are shaded; Ba atoms represented by circles.

Table VIII. Selected Interatomic Distanced (Å) for $Ba_3Nb_5O_{15}$, with Estimated Standard Deviations in Parentheses

Ba(1)–O(3)	2.878 (5)	4×	Nb(1)–O(1)	1.9887 (3)	2×
–O(5)	2.796 (3)	8×	–O(4)	1.965 (3)	4×
Ba(2)–O(1)	3.0401 (7)		Nb(2)–O(2)	1.982 (2)	
–O(2)	2.803 (5)	2×	–O(3)	1.9894 (3)	2×
–O(4)	2.867 (4)	4×	–O(4)	1.957 (5)	
			–O(5)	2.068 (5)	2×

$Nb_2^{5+}Nb_6^{2.67+}O_{14}^{2-}$, corresponding to 14 valence electrons/Nb_6 cluster. The Nb–Nb distances in the $[Nb_6O_{12}]O_6$ clusters vary considerably, between 2.751 and 2.879 Å, but the average Nb–Nb distance of 2.821 Å is again very close to that observed in other compounds containing this unit. This average appears to be limited to a narrow range (2.81–2.83 Å), independent from formal valence electron count and interconnectivity of the cluster units.

The main difference with the refinement in the *Cmca* space group reported earlier[18] is the ordered description of the B layer containing isolated NbO_6 octahedra. The higher symmetry C-centered space group generates Nb-atom positions with unusually short Nb–Nb distances (2.08 Å), necessitating a disordered description with 0.5 occupancy of each Nb site, and one oxygen with a very long Nb–O distance and large thermal parameters. After appropriate axis permutation, *Pcab* is a direct subgroup of *Cmca*, and after eliminating the (approximately 500) centering-violating reflections from our collected data set, refinement in spacegroup *Cmca* produced results identical with those reported previously.

$Ba_3Nb_5O_{15}$. From X-ray powder diffraction, $Ba_3Nb_5O_{15}$ was known to have a unit cell consistent with a tetragonal tungsten bronze (TTB) type structure.[14] This was confirmed by the single-crystal data (Figure 5). Selected interatomic distances and angles are listed in Table VIII. The structure strongly resembles that of the nonreduced (ferroelectric) compound $Ba_3TiNb_4O_{15}$[22] but crystallizes in the centrosymmetric space group $P4/mbm$, like the "parent" tetragonal tungsten bronze $K_3W_5O_{15}$.[34] Refinements in the noncentrosymmetric space groups $P4bm$ or $P\bar{4}b2$ did not yield any significant improvements, although

(34) Magneli, A. *Ark. Kemi* **1949**, *1*, 213.

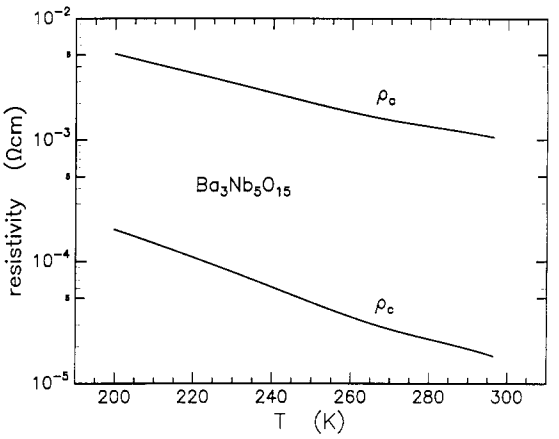

Figure 6. Single-crystal resistivity data for $Ba_3Nb_5O_{15}$.

no other checks for the presence of a center of symmetry were done. Refinement of the Ba occupancies showed no significant deviation from unity. This confirms the formulation of the compound in the ionic limit as $Ba_3^{2+}Nb^{4+}Nb_4^{5+}O_{15}^{2-}$, with an average Nb oxidation state of 4.8+. As observed in other TTB-type structures, one of the two crystallographically independent NbO_6 octahedra (Nb(2)) is more distorted, with Nb–O distances varying from 1.957 (5) to 2.068 (5) Å, compared to 1.965 (5) and 1.9887 (3) Å for Nb(1).

Physical Properties

$Ba_3Nb_5O_{15}$. Single-crystal resistivity data for $Ba_3Nb_5O_{15}$ between 200 and 300 K are shown in Figure 6. The resistivity is anisotropic, with $\rho_{\perp c} = 55\rho_{\parallel c}$ at 300 K. Despite the fairly low absolute resistivity ($\rho_{\parallel c} = 1.8 \times 10^{-5}$ Ω cm at 300 K), the resistivity has a negative temperature coefficient. From ln ρ vs $1/T$ plots activation energies of 0.131 eV ($\parallel$c) and 0.086 eV ($\perp$c) were determined. For pressed pellets an activation energy of 0.04 eV was reported for $T > 280$ K,[14] and semiconducting behavior was also noted for ceramic $Eu_3Nb_5O_{15}$, where Eu is formally divalent.[35] The observed slope of the ρ vs T plot for $Ba_3Nb_5O_{15}$ crystals varied somewhat for different samples, possibly indicating that this nearly metallic system is highly sensitive to impurities that can influence the carrier density (such as oxygen vacancies and incorporation of small amounts of Mo, though not enough as to be detected by standard methods such as X-ray fluorescence). In contrast, isostructural tetragonal tungsten bronzes exhibit a metallic temperature dependence of the resistivity, and a less pronounced anisotropy (e.g., $\rho_{\perp c} = 3.4\rho_{\parallel c}$ in $Na_{2.25}W_5O_{15}$[36]). For $Eu_3Nb_5O_{15}$, Raveau and Studer suggested, based on Goodenough's model for transition metal oxides,[37] that poor delocalization of Nb $4d_{xy}$ states, lowered below the conduction band (consisting of Nb $4d_{xz,yz}$ and O $2p_{x,y}$ orbitals) due to the tetragonal symmetry, combined with the relative small number of charge carriers (0.2 e/Nb, compare 0.45 e/W in $Na_{2.25}W_5O_{15}$[36]), could account for the small band gap semiconducting behavior of these TTB-type niobates.[35] If so, the reduced contribution of Nb $4d_{xy}$ orbitals to the conduction band could be a source for the observed strong anisotropy in the single-crystal resistivity of $Ba_3Nb_5O_{15}$.

$Ba_2Nb_{15}O_{32}$. Single-crystal resistivity measurements on $Ba_2Nb_{15}O_{32}$ between 100 and 540 K show semiconducting

(35) Studer, F.; Fayolle, J. P.; Raveau, B. *Mater. Res. Bull.* **1976**, *11*, 1125.
(36) Muhlestein, L. D.; Danielson, G. C. *Phys. Rev.* **1967**, *158*, 825.
(37) Goodenough, J. B. *Prog. Solid State Chem.* **1972**, *5*, 145.

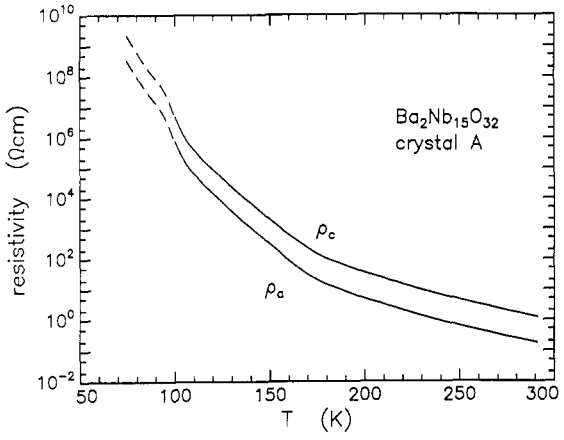

Figure 7. Single-crystal resistivity data for $Ba_2Nb_{15}O_{32}$. Data below 100 K are unreliable due to high sample and contact resistance.

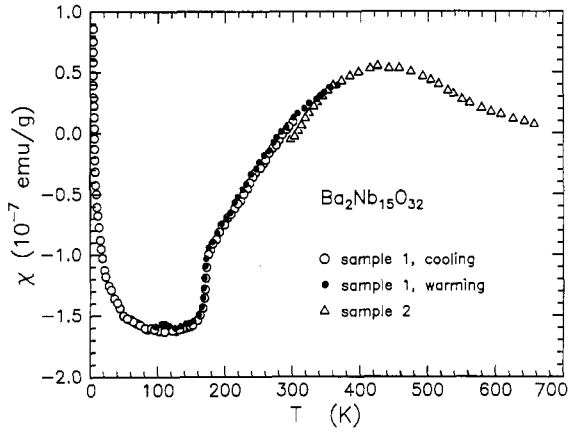

Figure 8. Magnetic susceptibility data (low temperature, circles; high temperature, triangles) for $Ba_2Nb_{15}O_{32}$. Uncorrected for Curie impurity "tail" and core diamagnetism.

behavior, and an anisotropy with $\rho_{\parallel c} = 6.7\rho_{\perp c}$ at 290 K. This makes it likely that the main conduction pathway is along the A layer (containing the 15-electron Nb_6 clusters and Nb(4)) in the *ab* plane. It may be noted that the Nb- -Nb distances between the A and B layers (minimal 3.65 Å) are significantly longer than those within the A layer (3.105 Å, Nb(3)–Nb(4)). The observed semiconducting behavior contrasts with the metallic conductivity observed in $NaNb_{10}O_{18}$,[30] in which a formal electron count also leads to 15 valence electrons/Nb_6 cluster. In that case a three-dimensional delocalization of the odd electron was proposed. Tight-binding calculations by Miller et al. on sheets of Nb_6 clusters sharing oxygens indicated that the Fermi level in a sheet of interconnected 16-electron clusters lies above that of the energy of the Nb d orbitals in free Nb atoms.[29] This could then account for the observed delocalization of a valence electron from the 15-electron clusters in $NaNb_{10}O_{18}$, accompanied by Pauli paramagnetism. The situation in $Ba_2Nb_{15}O_{32}$, in which the clusters are not directly linked through oxygen sharing, appears to be more complicated. The low-temperature single-crystal resistivity vs temperature graph (Figure 7) shows a semiconductor-to-semiconductor transition at 170 K. Magnetic susceptibility measurements on $Ba_2Nb_{15}O_{32}$ between 4 and 650 K (Figure 8, uncorrected for Curie "tail" and core diamagnetism) shows that this transition coincides with a magnetic transition from a weakly paramagnetic state to diamagnetism below the transition temperature. No significant hysteresis was observed in scanning across the transition in both temperature directions. A

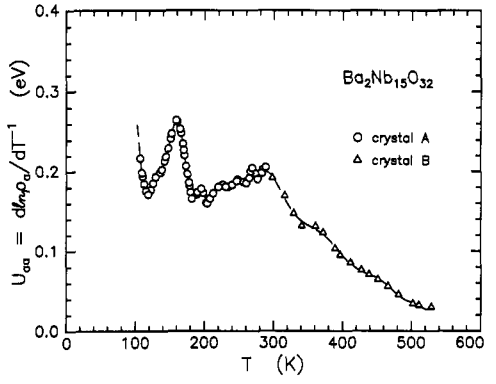

Figure 9. Plot of d ln ρ_a/dT^{-1} ("Arrhenius activation energy") versus T for single-crystal resistivity measurements on $Ba_2Nb_{15}O_{32}$. The anomaly at 170 K is associated with the semiconductor-to-semiconductor transition.

possible interpretation of these phenomena is that the odd electron in the 15-electron Nb_6 cluster is principally responsible for the observed conductivity, as well as the magnetism. Below 170 K, the compound apparently has a diamagnetic ground state. One possibility is that this is associated with a charge disproportionation, forming clusters with 14 and 16 valence electrons. In that case, the magnetic transition at 170 K may be associated with a spin-level crossing, as observed in the cluster compounds Nb_6I_{11} and HNb_6I_{11}.[38,39] However, in this case the state reached just above the transition temperature does not appear to be a simple localized high-spin state, as the susceptibility continues to increase linearly with T up to 300 K. Above 300 K the suceptibility begins to level off, reaching a maximum at 420 K, and eventually approaches Pauli paramagnetism at high temperatures. A plot of d ln ρ_a/dT^{-1} (U_{aa}, Arrhenius activation energy) versus temperature (Figure 9) shows that $Ba_2Nb_{15}O_{32}$ clearly is no simple activated intrinsic semiconductor, showing a drop in "activation energy" U_{aa} from 300 K upward (the region in which the susceptibility levels off), to a point where $U_{aa} < kT$. This suggests the presence of multiple states, associated with different magnetic moments, between the diamagnetic low-T ground state and a fully delocalized conducting state. The physical properties of $Ba_2Nb_{15}O_{32}$ are still under investigation. Preliminary low-temperature single-crystal X-ray diffraction has not so far revealed any discontinuous change in unit cell that might conceivably accompany a charge disproportionation to a diamagnetic ground state.

Conclusions

Low-volatility borate fluxes prove to be interesting media for the crystallization of reduced ternary early-transition-metal oxides under high-vacuum conditions. Use of the barium borate $BaO{\cdot}3B_2O_3$ as reagent and flux has enabled the isolation of single crystals of three different reduced barium niobates, of sufficient quality to allow single-crystal X-ray structure determinations and resistivity measurements. As the formation of $Ba_2Nb_{15}O_{32}$ has shown, it is possible to obtain new phases by this method. Results in the Sr–Nb–O, Sr–Ti–O, and La–Ti–O systems[40,41] suggest that this technique is more generally

(38) Finley, J. J.; Nohl, H.; Vogel, E. E.; Imoto, H.; Camley, R. E.; Zevin, V.; Anderson, O. K.; Simon, A. *Phys. Rev. Lett.* **1981**, *46*, 1472.
(39) Imoto, H.; Simon, A. *Inorg. Chem.* **1982**, *21*, 308.
(40) Hessen, B.; Sunshine, S. A.; Siegrist, T.; Fiory, A. T. In *Chemistry of Electronic Ceramic Materials*; Davies, P. K., Roth, R. S., Eds.; NIST special publication 804, 1991; p 237.
(41) Hessen, B.; Sunshine, S. A.; Siegrist, T.; Jimenez, R. *Mater. Res. Bull.* **1991**, *26*, 85.

applicable to alkaline-earth-metal and lanthanide compounds of reduced early transition metals.

Acknowledgment. We thank R. M. Fleming, L. F. Schneemeyer, and T. T. Palstra for stimulating discussions. B.H. thanks the Netherlands Organization for Scientific Research (NWO) for the award of a fellowship.

Supplementary Material Available: Details of the X-ray structure determinations and list of positional and anisotropic thermal parameters (7 pages); listing of observed and calculated structure factors (30 pages).

^{7}Li NMR Study of Polymer Electrolytes Based on Composites of Poly[bis((methoxyethoxy)ethoxy)phosphazene] and Poly(ethylene oxide)

K. J. Adamic and S. G. Greenbaum*

Department of Physics, Hunter College of CUNY, New York, New York 10021

K. M. Abraham* and M. Alamgir

EIC Laboratories Inc., 111 Downey St., Norwood, Massachusetts 02062

M. C. Wintersgill and J. J. Fontanella*

Department of Physics, U.S. Naval Academy, Annapolis, Maryland 21402

Received January 2, 1991. Revised Manuscript Received March 25, 1991

Polymer electrolytes consisting of mixtures of poly[bis((methoxyethoxy)ethoxy)phosphazene] (MEEP) and poly(ethylene oxide) (PEO) or poly(propylene oxide) (PPO) complexed with $LiClO_4$ or $LiBF_4$ have been studied by differential scanning calorimetry (DSC) and ^{7}Li nuclear magnetic resonance (NMR) spectroscopy. Both types of measurements demonstrate that the MEEP/PEO composites are multiphase in that amorphous MEEP-like and crystalline PEO-like phases are present in the samples. The NMR results show that significant Li^+ ion mobility in the MEEP-like phase occurs only above the lowest temperature glass transition as indicated by DSC measurements. Strong cation–anion association effects are suggested by dipolar broadening in BF_4^- containing materials and by precipitation of salt crystallites from the MEEP/PPO composite at elevated temperature.

Introduction

Poly(ethylene oxide) (PEO) and its alkali metal salt complexes have played an important role in the development of polymeric solid electrolytes intended for use in high-energy-density batteries.[1-3] PEO complexes are generally multiphase with regard to the coexistence of crystalline and amorphous phases in the same sample. A serious limitation of PEO–alkali metal salt complexes that is related to the presence of the crystalline phase is their relatively low ionic conductivity below approximately 60 °C. Recognition of the fact that significant ion transport in polymer electrolytes occurs only in the rubbery phase of the amorphous component (above its glass transition temperature, T_g) has led to the synthesis of a variety of elastomeric complexes with low T_g's.[4-6] One such material is poly[bis((methoxyethoxy)ethoxy)phosphazene] (MEEP), which combines the highly ion solvating property of its ethylene oxide side groups with the elastomeric character imparted by the flexible polyphosphazene backbone.[4]

Efforts to improve the mechanical stability of MEEP have included chemical[7] and radiation[8] crosslinking. Recently, two of us have described the synthesis and study of composites of MEEP and PEO complexed with lithium salts.[9] These materials were found to possess the mechanical integrity of PEO–salt complexes while offering significantly higher room-temperature conductivity.

Nuclear magnetic resonance (NMR) has been shown to be a powerful technique in probing the dynamical behavior of ions in solid electrolytes in general[10] and polymer electrolytes in particular.[11,12] This paper describes the use of ^{7}Li NMR to investigate both the distribution and temperature-dependent mobility of Li ions in MEEP/PEO

(1) Wright, P. V. *Br. Polym. J.* **1975**, *7*, 319.
(2) Armand, M. B.; Chabagno, J. M.; Duclot, M. J. In *Fast Ion Transport in Solids*; Vashishta, P., Mundy, J. N., Shenoy, G. K., Eds.; Elsevier North-Holland: New York, 1979; p 131.
(3) MacCallum, J. R., Vincent, C. A., Eds. *Polymer Electrolyte Reviews*; Elsevier Applied Science: London, 1987, 1989; Vols 1, 2.
(4) Blonsky, P. M.; Shriver, D. F.; Austin, P.; Allcock, H. R. *J. Am. Chem. Soc.* **1984**, *106*, 6854.
(5) Bouridah, A.; Dalard, F.; Deroo, D.; Cheradame, H.; LeNest, J. F. *Solid State Ionics* **1985**, *15*, 233.
(6) Greenbaum, S. G.; Pak, Y. S.; Adamic, K. J.; Wintersgill, M. C.; Fontanella, J. J.; Beam, D. A.; Mei, H. L.; Okamoto, Y. *Mol. Cryst. Liq. Cryst.* **1988**, *160*, 347.
(7) Tonge, J. S.; Shriver, D. F. *J. Electrochem. Soc.* **1987**, *134*, 269.
(8) Nazri, G.; Meibuhr, S. P. In *Materials and Processes for Lithium Batteries*; Abraham, K. M.; Owens, B. B., Eds.; The Electrochemical Society: Pennington, NJ, 1989; **PV89-4**, p 332.
(9) Abraham, K. M.; Alamgir, M.; Reynolds, R. K. *J. Electrochem. Soc.* **1989**, *136*, 3576.
(10) Brinkmann, D. *Solid State Ionics* **1981**, *5*, 53.
(11) Berthier, C.; Gorecki, W.; Minier, M.; Armand, M. B.; Chabagno, J. M.; Rigaud, P. *Solid State Ionics* **1983**, *11*, 91.
(12) Greenbaum, S. G.; Pak, Y. S.; Wintersgill, M. C.; Fontanella, J. J. *Solid State Ionics* **1988**, *31*, 241.

0897-4756/91/2803-0534$02.50/0